Multiple mechanisms for stochastic resonance are inherent to sinusoidally driven noisy Hopf oscillators

Dáibhid Ó Maoiléidigh*

Department of Otolaryngology–Head and Neck Surgery, Stanford University School of Medicine, Stanford, CA 94305, USA and Laboratory of Sensory Neuroscience, The Rockefeller University, New York, NY 10065, USA

(Received 2 November 2017; published 28 February 2018)

To ensure their sensitivity to weak periodic signals, some physical systems likely operate near a Hopf bifurcation. Many systems operating near such a bifurcation exhibit stochastic resonance, but it is unclear which mechanisms for resonance are inherent to the bifurcation. To address this question, we study the *sinusoidally forced* dynamics of noisy supercritical and subcritical Hopf oscillators. We find four qualitatively different mechanisms for stochastic resonance and determine the conditions for each type of resonance.

DOI: 10.1103/PhysRevE.97.022226

I. INTRODUCTION

To achieve great sensitivity to sinusoidal stimuli, it has been proposed that some natural systems possessing a supercritical Hopf bifurcation operate close to the bifurcation [1]. The sensitivity of such systems may be limited by noise, but it is also possible that noise enhances their responsiveness in certain situations. Stochastic resonance, broadly speaking, is the peaking of a system's response to a deterministic stimulus as a function of the noise level [2,3]. Therefore, we would like to know the mechanisms for stochastic resonance intrinsic to systems operating near a Hopf bifurcation.

Numerous studies have explored the response to periodic forcing of particular types of oscillators that operate near a Hopf bifurcation. For illustration, near a supercritical Hopf bifurcation, the FitzHugh-Nagumo model [3,4], an electron-hole plasma model [5], and the Brusselator model [6] exhibit stochastic resonance that is related to an abrupt increase in the amplitude of self-oscillation as a function of a control parameter. In contrast, stochastic resonance in the Noyes-Field-Thomson model [7], the Hindmarsh-Rose model [8], a model of intracellular Ca^{2+} oscillations [9], and a biogeochemical climate model [10] is associated with spontaneous oscillations of finite amplitude that occur at a subcritical Hopf bifurcation. The effects of noise are sometimes model dependent and sometimes attributed to the bifurcations. For example, because the supercritical Hopf normal form does not produce autonomous oscillations that rise sharply with control parameter, the specific type of stochastic resonance associated with the abrupt rise described above cannot be intrinsic to this bifurcation.

To determine the behaviors of noisy sinusoidal-signal detectors that are inherent to Hopf bifurcations, we study the response to sinusoidal forcing of the supercritical and subcritical Hopf normal forms in the presence of additive complex Gaussian white noise with uncorrelated components. These Langevin equations define noisy Hopf oscillators, for which there is an equivalent formulation in terms of Fokker-Planck equations. Analytical and numerical solutions of the Fokker-Plank equations allow us to determine the responsiveness of a Hopf oscillator to sinusoidal forcing over a large range of noise levels. By relating changes in the probability density as a function of the noise level to the phase-locked amplitude and the degree of entrainment, we find several mechanisms for stochastic resonance.

II. HOPF OSCILLATORS WITH ADDITIVE NOISE

The Hopf normal form in the presence of sinusoidal forcing with additive white noise possessing uncorrelated real and imaginary components is

$$\dot{z} = (\mu + i\omega_0)z + (b + ib')|z|^2 z + (c + ic')|z|^4 z + f e^{i(\omega t+\theta)} + \eta, \tag{1}$$

in which μ is the control parameter, ω_0 is the Hopf frequency, and b, b', c, and c' are coefficients defining the system's nonlinearity [11–13]. The complex forcing term $F(t) = f e^{i(\omega t+\theta)}$ has amplitude f, frequency ω, and phase θ. The noise $\eta(t)$ is complex and white and satisfies $\langle \eta(t) \rangle = 0$, $\langle \eta(t)\eta(t') \rangle = 0$, and $\langle \eta(t)\eta^\dagger(t') \rangle = 4d\delta(t - t')$, in which $\langle\rangle$ represents the ensemble average, $\eta^\dagger(t)$ is the complex conjugate of $\eta(t)$, and d is the strength of the noise [14–16].

In the deterministic limit, a Hopf bifurcation occurs at $\mu = 0$; the system oscillates for $\mu > 0$ and possesses a stable fixed point when $\mu < 0$. In the case of a supercritical Hopf bifurcation, $b < 0$, $c = 0$, and the amplitude of self-oscillation grows continuously from zero at the bifurcation. At a subcritical Hopf bifurcation, which occurs when $b > 0$ and $c < 0$, oscillations of nonzero amplitude exist. A saddle node of limit-cycle bifurcation generates the oscillations at $\mu = \frac{b^2}{4c} < 0$. When $\frac{b^2}{4c} < \mu < 0$, a stable fixed point is enclosed by an unstable limit cycle, which is in turn encircled by a stable limit cycle. We call the cases with $\mu > 0$ the oscillatory sides of the bifurcations and refer to the supercritical situation of $\mu < 0$ and subcritical case of $\mu < \frac{b^2}{4c}$ as the quiescent sides of the bifurcations.

*dmelody@stanford.edu

In the rotating frame of the forcing, Eq. (1) can be rewritten as

$$\dot{y} = (\mu - i\delta\omega)y + (b + ib')|y|^2 y + (c + ic')|y|^4 y + f + \eta e^{-i(\omega t+\theta)}, \tag{2}$$

in which $y \equiv ze^{-i(\omega t+\theta)}$ and $\delta\omega \equiv \omega - \omega_0$ is the frequency detuning. For complex Gaussian noise, for which the real and imaginary components are Gaussian distributed with variance $2d$, the probability density $P(y,t)$ for y satisfies the Fokker-Planck equation:

$$\begin{aligned}\partial_t P = &-\partial_R[(\mu y_R + \delta\omega y_I + (by_R - b'y_I)\rho^2 \\ &+ (cy_R - c'y_I)\rho^4 + f)P - d\partial_R P] \\ &- \partial_I[(\mu y_I - \delta\omega y_R + (by_I + b'y_R)\rho^2 \\ &+ (cy_I + c'y_R)\rho^4)P - d\partial_I P],\end{aligned} \tag{3}$$

in which $y \equiv y_R + iy_I$, $\partial_R \equiv \partial/\partial y_R$, $\partial_I \equiv \partial/\partial y_I$, and the radial coordinate $\rho(y_R, y_I) \equiv \sqrt{y_R^2 + y_I^2}$ [14,17].

The response of a supercritical Hopf oscillator to sinusoidal forcing can be multivalued when b' is nonzero and the response of a subcritical oscillator is likely more complicated [18,19]. To determine the most basic consequences of noise for a forced Hopf oscillator, we limit our analysis to the case of $b' = 0$ and $c' = 0$, which defines an isochronous Hopf oscillator [20].

Because the steady-state solution to Eq. (3) determines whether stochastic resonance occurs, it is instructive to first discuss the solution as a function of the conditions.

A. The position distribution

1. Tuned forcing

The steady-state distribution $P_s(y)$ of y in the case of zero detuning, $\delta\omega = 0$, is given by

$$P_s = Ne^{\alpha/d}, \tag{4}$$

in which N is a normalization constant and $\alpha = \mu\rho^2/2 + b\rho^4/4 + c\rho^6/6 + fy_R$. The solution for the supercritical case has been reported previously [14] and the unforced solution for both types of bifurcations has been discussed [21,22]. In the original frame of reference, the distribution $P_{zs}(z,t)$ for z rotates at the frequency of driving and is given by

$$P_{zs} = N\exp\left\{\frac{\mu\rho^2}{2d} + \frac{b\rho^4}{4d} + \frac{c\rho^6}{6d} + \frac{f[z_R\cos(\omega_0 t + \theta) + z_I \sin(\omega_0 t + \theta)]}{d}\right\}. \tag{5}$$

When $f = 0$, the steady-state distribution P_s is radially symmetric and has radial maxima at values of $\sqrt{y_R^2 + y_I^2} = \rho_m$ satisfying $c\rho_m^5 + b\rho_m^3 + \mu\rho_m = 0$ and $5c\rho_m^4 + 3b\rho_m^2 + \mu < 0$, that is, at the same loci as the stable manifolds of the deterministic system. A change in the qualitative shape of a system's state distribution is known as a phenomenological bifurcation (Fig. 1) [23]. Here the phenomenological bifurcations coincide with the deterministic bifurcations independent of the noise level d.

In the unforced case, the steady-state distribution in a frame rotating at $\omega = \omega_0$ for the radius ρ and the phase difference $\psi \equiv \phi - \omega t - \theta$ is $P_{ps}(\rho,\psi) \equiv \rho P_s(y(\rho,\psi))$, such that $y = \rho e^{i\psi}$. In this coordinate system, the radial distribution's maxima depend on d and occur at values of $\rho = \rho_m$ satisfying $c\rho_m^6 + b\rho_m^4 + \mu\rho_m^2 + d = 0$ and $7c\rho_m^6 + 5b\rho_m^4 + 3\mu\rho_m^2 + d < 0$. The radial distribution is unimodal in the supercritical case. In the subcritical case, the distribution is bimodal for $\mu_1(b,c,d) < \mu < \mu_2(b,c,d) < 0$ and $d < b^3/27c^2$ and unimodal otherwise, in which $\mu = \mu_{1,2}(b,c,d)$ are solutions of $4b^3d + 27c^2d^2 - 18bcd\mu - b^2\mu^2 + 4c\mu^3 = 0$.

Forcing at the resonant frequency breaks the radial symmetry of the Cartesian distributions, although they retain reflection symmetry around the line $y_I = 0$. There is a preferred phase difference of zero between the forcing and the oscillator's response such that the most probable value for y_I is zero (Fig. 1). Due to the simple form of the noise, the qualitative shape of the forced position distribution is unaffected by the noise level d and depends only on the fixed points of the deterministic system. The extrema of the distribution P_s along the symmetry line $y_I = 0$ are given by

$$\frac{\partial P_s(y_R,0)}{\partial y_R} = 0 \tag{6}$$

and satisfy the fixed point condition [Eq. (A4) in the Appendix]. Each stable response to tuned forcing corresponds to a peak in P_s.

In the supercritical case, Eq. (A4) defines a single fixed point when $\mu < 0$ or $f > \sqrt{-4\mu^3/27b}$ and three fixed points for $f < \sqrt{-4\mu^3/27b}$ when $\mu > 0$; a stable fixed point, at which the distribution P_s is a maximum, an unstable fixed point, and a saddle point. The stable fixed point and the saddle point are at antipodal ends of a ring-shaped crater exhibited by P_s. The saddle point and unstable fixed point vanish for large forces through a saddle-node bifurcation, corresponding to the loss of the crater in P_s. When $\mu < 0$, P_s has a single maximum at the only stable fixed point. The most probable value for y_R is $y_{Rm} = (-f/b)^{1/3}$ when $\mu = 0$. The most probable value y_{Rm} is less than $(-f/b)^{1/3}$ and increases with f more slowly than $f^{1/3}$ when $\mu < 0$, whereas the opposite is true when $\mu > 0$. Irrespective of the value of μ, however, $y_{Rm} \to (-f/b)^{1/3}$ as $f \to \infty$.

The subcritical distribution has four qualitatively dissimilar shapes associated with different sets of fixed points defined by Eq. (A4) (Fig. 2). In the range $9b^2/20c < \mu < 0$, the subcritical Hopf oscillator has two maxima for tuned sinusoidal forcing satisfying $f_1(\mu,b,c) < f < f_2(\mu,b,c)$, in which

$$\begin{aligned} f_1(\mu,b,c) &= \sqrt{\frac{-3b - \sqrt{9b^2 - 20c\mu}}{10c}}\left(\frac{3b^2 - 20c\mu + b\sqrt{9b^2 - 20c\mu}}{25c}\right) \quad \text{for} \quad \mu < \frac{b^2}{4c}, \quad \text{and} \\ f_2(\mu,b,c) &= \sqrt{\frac{-3b + \sqrt{9b^2 - 20c\mu}}{10c}}\left(\frac{3b^2 - 20c\mu - b\sqrt{9b^2 - 20c\mu}}{25c}\right). \end{aligned} \tag{7}$$

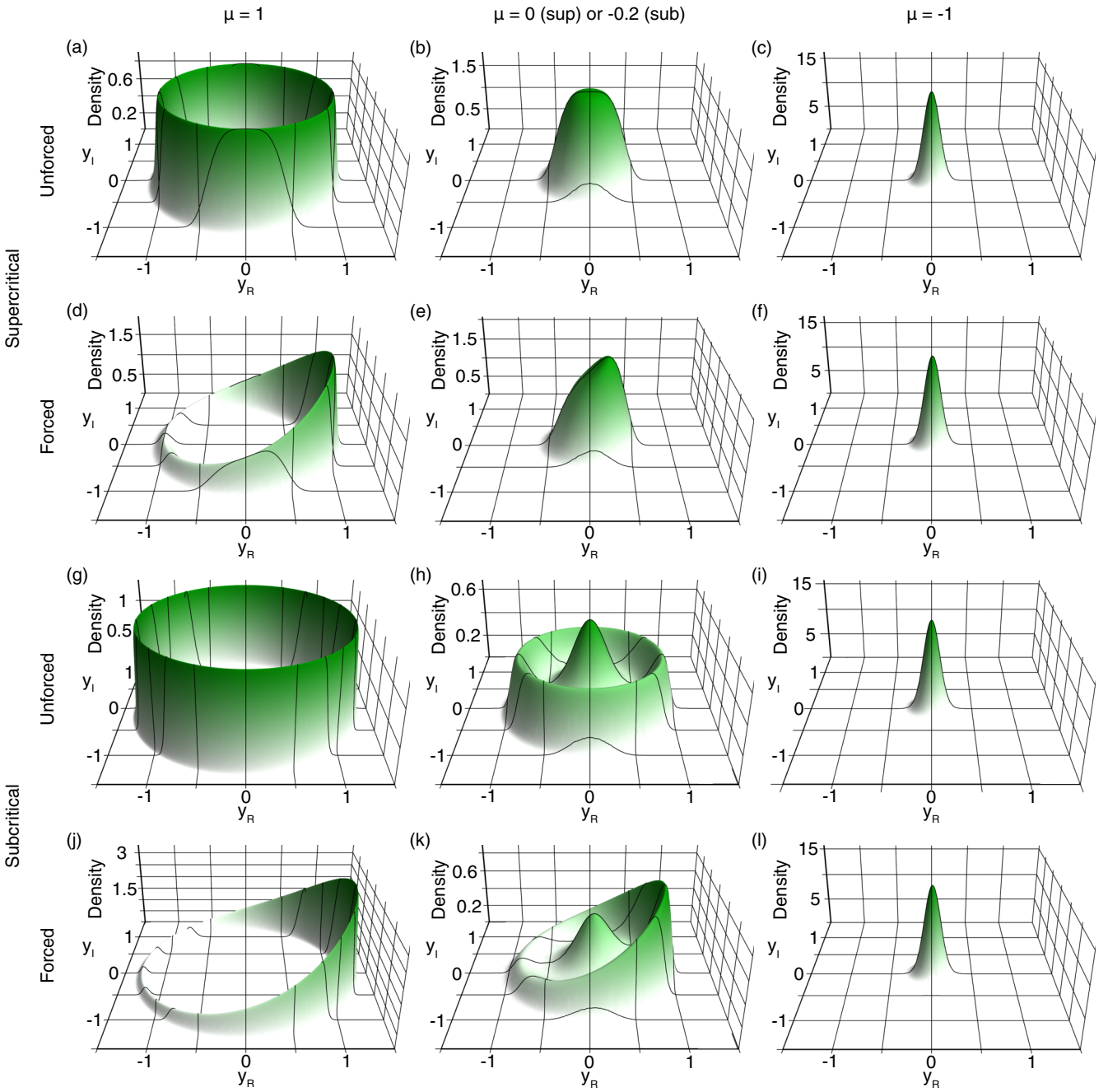

FIG. 1. Steady-state distributions of probability density are shown for stochastic Hopf oscillators in a frame rotating at the forcing frequency for different values of the control parameter μ in unforced $f = 0$ and forced $f = 10^{-2}$ scenarios [Eq. (4)]. Forcing is at the Hopf frequency $\omega = \omega_0$ and the noise level $d = 10^{-2}$. In the absence of forcing, the distributions are radially symmetric. Forcing introduces radial asymmetry and a most probable phase of 0 radians. In these cases, the corresponding distributions in the original frame of reference rotate in a counterclockwise direction around the origin at the frequency of driving. [(a)–(f)] Supercritical Hopf oscillator (sup). [(g)–(l)] Subcritical Hopf oscillator (sub). For all figures in this manuscript the Hopf frequency $\omega_0 = 1$, $b = -1$, and $c = 0$ in the supercritical case or $b = 1$ and $c = -1$ in the subcritical case.

Within this region, two stable fixed points, two saddle points, and an unstable fixed point yield a distribution with two maxima and a crater for $f < f_3(\mu,b,c)$, in which

$$f_3(\mu,b,c) = \sqrt{\frac{-3b - \sqrt{9b^2 - 20c\mu}}{10c}}\left(\frac{3b^2 - 20c\mu + b\sqrt{9b^2 - 20c\mu}}{25c}\right) \quad \text{for} \quad \mu > \frac{b^2}{4c}. \tag{8}$$

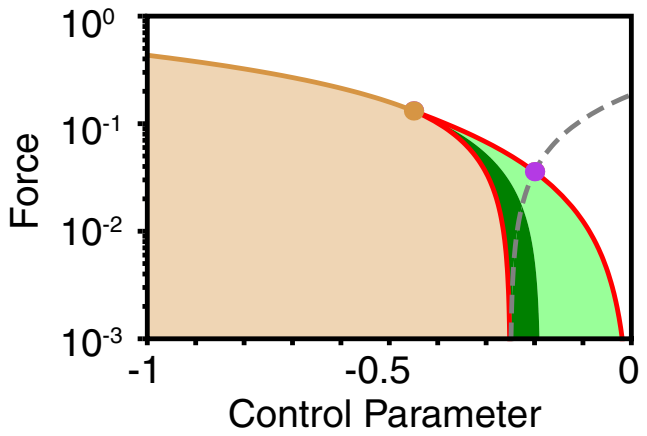

FIG. 2. The state diagram for a deterministic subcritical Hopf oscillator subjected to resonant forcing is shown. Global bifurcations are not shown. There exist two stable responses to tuned forcing with amplitude f for operating points within the green region demarcated by the red saddle-node bifurcation lines [$f_1(\mu,b,c) < f < f_2(\mu,b,c)$] that intersect at a cusp bifurcation [$\mu = 9b^2/20c$ and $f = \sqrt{-54b^5/3125c^3}$, orange dot]. Two unstable fixed points arise through a third saddle-node bifurcation line [gray dashed, $f_3(\mu,b,c)$] that intersects one of the red lines at $\mu = b^2/5c$ and $f = \sqrt{-4b^5/3125c^3}$ (purple dot) and asymptotically meets the other red line at $\mu = b^2/4c$ and $f = 0$. Stochastic resonance in the phase-locked amplitude and the vector strength occurs for operating points in the region shaded dark green, in which $\alpha_1 < \alpha_2$. The phase-locked amplitude also peaks as a function of the noise level for points in the region shaded orange [$f < f_1(\mu,b,c)$ and $9b^2/20c < \mu < b^2/4c$ or $f < f_4(\mu,b,c)$ and $\mu < 9b^2/20c$].

When $f > f_3(\mu,b,c)$, two stable fixed points and a saddle point correspond to two maxima and no crater. Outside of the two stable-solution region, there is one stable fixed point and no crater for $f > \max(f_2(\mu,b,c), f_3(\mu,b,c))$ or $\mu < 9b^2/20c$. In the case of $\mu > b^2/5c$ and $f_2(\mu,b,c) < f < f_3(\mu,b,c)$, a stable fixed point, a saddle point, and an unstable fixed point correspond to a distribution possessing one maximum and a crater. In every case, the location of the distribution's peak y_{Rm} rises as μ grows, and $y_{\mathrm{Rm}} \to (-f/c)^{1/5}$ as $f \to \infty$ for all values of μ.

In polar coordinates, the radial maxima occur at values of ρ_{m} satisfying $c\rho_{\mathrm{m}}^6 + b\rho_{\mathrm{m}}^4 + \mu\rho_{\mathrm{m}}^2 + f\rho_{\mathrm{m}} + d = 0$ and $7c\rho_{\mathrm{m}}^6 + 5b\rho_{\mathrm{m}}^4 + 3\mu\rho_{\mathrm{m}}^2 + 2f\rho_{\mathrm{m}} + d < 0$. In contrast to the Cartesian distribution, the most probable value for the radius and the modality of the radial distribution depend on the noise level. In agreement with a previous calculation for the supercritical case [16], $P_{\mathrm{ps}} = P_{\mathrm{ps0}}[1 + f\rho\cos(\psi)/d]$ to linear order in f, in which P_{ps0} is the steady-state polar distribution for $f = 0$.

2. Detuned forcing

A closed-form solution for Eq. (3) is not apparent when $\delta\omega \neq 0$, but we can solve for the steady-state distribution numerically by employing P_{s} to set initial and boundary conditions [Eq. (4)]. We find the distribution $P_{\mathrm{p}}(\rho,\psi,t)$ in polar coordinates with periodic boundary conditions in the phase coordinate $P_{\mathrm{p}}(\rho,2\pi,t) = P_{\mathrm{p}}(\rho,0,t)$ and $\partial_\psi P_{\mathrm{p}}(\rho,\psi,t)|_{\psi=2\pi} = \partial_\psi P_{\mathrm{p}}(\rho,\psi,t)|_{\psi=0}$. In the radial direction we use the Dirichlet boundary condition $P_{\mathrm{p}}(\rho_{\max},\psi,t) = P_{\mathrm{ps}}(\rho_{\max},\psi)$, in which $P_{\mathrm{ps}}(\rho,\psi) = \rho P_{\mathrm{s}}(y(\rho,\psi))$ is the steady-state solution for zero detuning in polar coordinates. The maximum value for ρ is selected such that $P_{\mathrm{ps}}(\rho_{\max},\psi) \approx 0$. The initial condition is chosen to be $P_{\mathrm{p}}(\rho,\psi,0) = P_{\mathrm{ps}}(\rho,\psi)$.

The polar Fokker-Plank equation possesses terms that diverge as $\rho \to 0$,

$$\partial_t P_{\mathrm{p}} = -\partial_\rho\left[\left(\mu\rho + b\rho^3 + c\rho^5 + f\cos\psi + \frac{d}{\rho}\right)P_{\mathrm{p}} - d\partial_\rho P_{\mathrm{p}}\right] - \partial_\psi\left[\left(-\delta\omega + b'\rho^2 + c'\rho^4 - \frac{f\sin\psi}{\rho}\right)P_{\mathrm{p}} - \frac{d}{\rho^2}\partial_\psi P_{\mathrm{p}}\right]. \tag{9}$$

To circumvent numerical complications arising from these divergences, we define a minimum value for ρ, $\rho_{\min}$, and use the condition $P_{\mathrm{p}}(\rho_{\min},\psi,t) = P_{\mathrm{ps}}(\rho_{\min},\psi)$, in which $P_{\mathrm{ps}}(\rho_{\min},\psi) \approx 0$. The distribution is normalized at the end of the integration time $t_{\max}$ to have unit volume over the annulus defined by $\rho \in [\rho_{\min},\rho_{\max}]$ and $\psi \in [0,2\pi]$. The steady-state distribution in Cartesian coordinates is then given by $P_{\mathrm{s}\delta\omega}(y) = P_{\mathrm{p}}(\rho(y),\psi(y),t_{\max})/\rho(y)$, in which $t_{\max}$ is chosen such that $P_{\mathrm{s}\delta\omega}(y)$ has converged sufficiently.

Forcing at a frequency different from the Hopf frequency breaks the Cartesian distribution's reflection symmetry (Fig. 3). In contrast to the tuned case, peaks of the steady-state distribution do not reside at the stable fixed points and instead their positions depend on the value of the noise level d. For negative detuning, the probability density is rotated counterclockwise such that its peak leads the forcing. This result accords qualitatively with the deterministic limit, in which a stable response of an oscillator to periodic driving at a frequency below the Hopf frequency leads the input [20]. The phase lead of the distribution's peak also occurs, however, when there is no stable fixed-point response in the deterministic limit. Similarly to the stable response in the absence of noise, the oscillator's most probable position lags the forcing for positive detuning. Raising the noise level drives the peak's phase to zero and broadens the distribution. For increasing noise, the detuned distribution approaches the tuned case. A moderate noise level nonetheless produces detuned distributions that are less skewed than those corresponding to tuned forcing.

The deterministic response to weak detuned forcing is aperiodic whenever the ratio of the forcing frequency to the Hopf frequency is irrational and does not approach a steady state in any reference frame [20]. In contrast, the stochastic system possesses a steady-state position distribution for any driving frequency in a reference frame rotating at that frequency. Unlike the tuned situation, however, the effect of detuned forcing on the distributions declines as the control parameter μ rises.

B. Stochastic resonance

1. Phase-locking to tuned forces can peak as a function of the noise level near subcritical but not supercritical Hopf bifurcations

Because we wish to distinguish an oscillator's response to sinusoidal input from that provoked by noise, we employ the

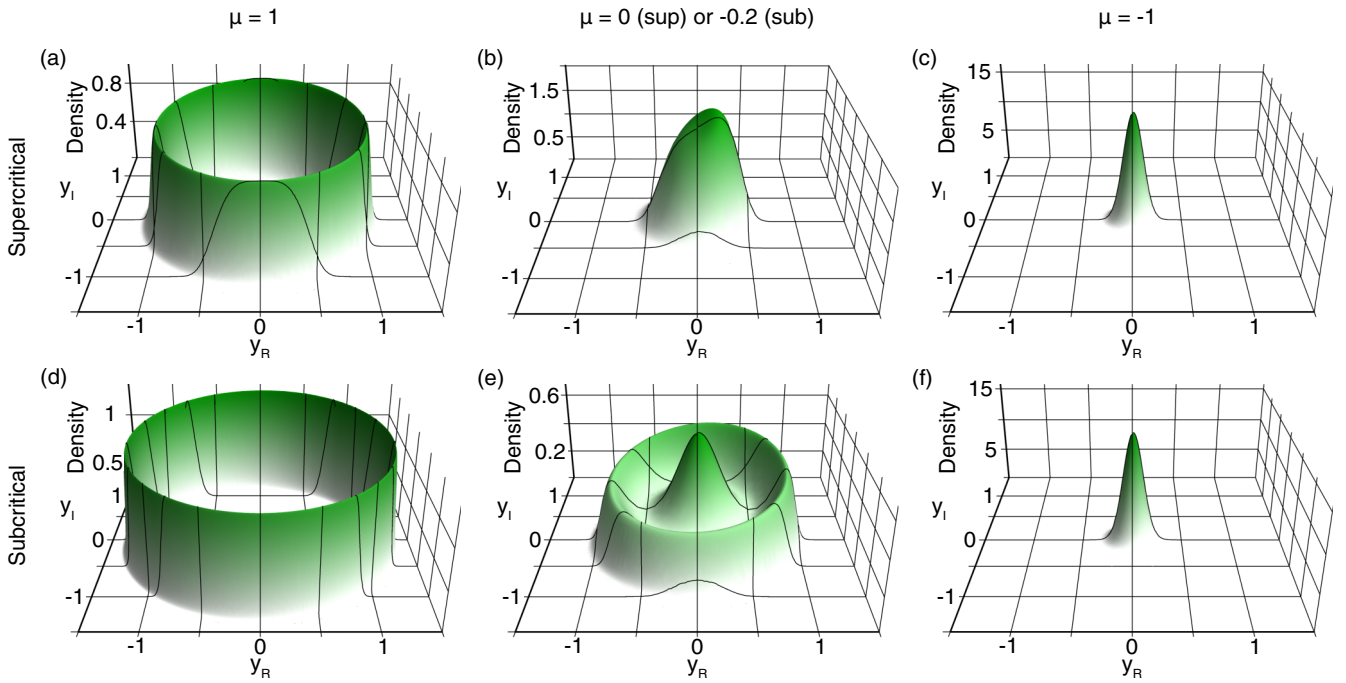

FIG. 3. Steady-state distributions of probability density for stochastic Hopf bifurcations are shown for a frame rotating at the forcing frequency for different values of the control parameter μ. Forcing is at a frequency, $\omega = 0.9\,\omega_0$, lower than the Hopf frequency ω_0, and has an amplitude $f = 10^{-2}$; the noise level $d = 10^{-2}$. The distributions are rotated counterclockwise and are less skewed than the distributions resulting from forcing at the Hopf frequency (Fig. 1). [(a)–(c)] Supercritical Hopf oscillator (sup). [(d)–(f)] Subcritical Hopf oscillator (sub).

phase-locked amplitude

$$|\langle\tilde{z}(\omega)\rangle_{zs}| = |\langle y\rangle_s| \tag{10}$$

and the vector strength

$$V \equiv \left|\lim_{T\to\infty}\frac{1}{T}\int_0^T e^{i\psi(t)}\,dt\right| = |\langle e^{i\psi}\rangle_s|, \tag{11}$$

in which ω is the stimulus frequency, $\tilde{z}$ is the finite-time Fourier transform of z, and $\langle\rangle_{zs}$ and $\langle\rangle_s$ denote long-time ensemble averages in the respectively nonrotating and rotating frames. In the presence of noise, the phase-locked amplitude and the vector strength are nonzero only if the forcing amplitude $f \neq 0$.

Suppose we would like to determine if $|\langle g\rangle|$ peaks as a function of the noise level d, in which $g = g_R(y_R, y_I) + i g_I(y_R, y_I)$. Extrema of $|\langle g\rangle|$ occur when

$$\frac{\partial|\langle g\rangle|}{\partial d} = 0 \quad \text{or equivalently when} \quad \frac{\partial(\langle g_R\rangle + \langle g_I\rangle)}{\partial d} = 0. \tag{12}$$

For tuned forcing, $P_s = N\exp(\alpha/d)$ resulting in

$$\frac{\partial(\langle g_R\rangle_s + \langle g_I\rangle_s)}{\partial d} = -\frac{\mathrm{cov}(g_R + g_I,\alpha)}{d^2}, \tag{13}$$

in which $\mathrm{cov}(g,\alpha) = \langle g\alpha\rangle_s - \langle g\rangle_s\langle\alpha\rangle_s$ is the covariance under the distribution P_s. Maxima of $|\langle g\rangle_s|$ occur when

$$\mathrm{cov}(g_R + g_I,\alpha) = 0 \quad \text{and} \quad \mathrm{cov}(g_R + g_I,\alpha^2) < 0. \tag{14}$$

If $g_I \to -g_I$ as $y_I \to -y_I$, then $\mathrm{cov}(g_I,\alpha) = 0$ and $\mathrm{cov}(g_I,\alpha^2) = 0$. Correspondingly,

$$\frac{\partial|\langle y\rangle_s|}{\partial d} = -\frac{\mathrm{cov}(y_R,\alpha)}{d^2} \quad \text{and} \tag{15}$$

$$\frac{\partial|\langle e^{i\psi}\rangle_s|}{\partial d} = -\frac{\mathrm{cov}(y_R/\rho,\alpha)}{d^2}, \tag{16}$$

such that the phase-locked amplitude peaks when

$$\mathrm{cov}(y_R,\alpha) = 0 \quad \text{and} \quad \mathrm{cov}(y_R,\alpha^2) < 0, \tag{17}$$

and the vector strength is a maximum for

$$\mathrm{cov}(y_R/\rho,\alpha) = 0 \quad \text{and} \quad \mathrm{cov}(y_R/\rho,\alpha^2) < 0. \tag{18}$$

The fact that conditions Eqs. (17) and (18) differ implies that if the responsiveness measures peak they generally do so at different noise levels.

Because the phase-locked amplitude and vector strength tend to zero as the noise level increases to infinity, they must peak if they increase for some finite d. If the phase-locked amplitude peaks at d_1, then

$$\mathrm{cov}(y_R,\alpha) < 0 \tag{19}$$

at some $d < d_1$, whereas if the vector strength peaks at d_2, then

$$\mathrm{cov}(y_R/\rho,\alpha) < 0 \tag{20}$$

at some $d < d_2$. Stochastic resonance does not occur for a resonantly forced supercritical Hopf oscillator but is possible for a subcritical Hopf oscillator under certain conditions (Fig. 4).

To find analytical conditions for stochastic resonance, we consider the limit of small noise. For small $d \neq 0$, the

distribution $P_s = N\exp(\alpha/d)$ is sharply peaked around its maxima y_m that satisfy

$$\left.\frac{\partial\alpha}{\partial y_R}\right|_{y_m} = 0 \quad \text{and} \quad \left.\frac{\partial^2\alpha}{\partial y_R^2}\right|_{y_m} < 0, \tag{21}$$

$$\left.\frac{\partial\alpha}{\partial y_I}\right|_{y_m} = 0 \quad \text{and} \quad \left.\frac{\partial^2\alpha}{\partial y_I^2}\right|_{y_m} < 0, \tag{22}$$

which yield

$$cy_{Rm}^5 + by_{Rm}^3 + \mu y_{Rm} + f = 0 \quad \text{and} \quad 5cy_{Rm}^4 + 3by_{Rm}^2 + \mu < 0, \tag{23}$$

$$y_{Im} = 0 \quad \text{and} \quad y_{Rm} > 0. \tag{24}$$

These equations also define the stable fixed points of the deterministic system with eigenvalues $5cy_{Rm}^4 + 3by_{Rm}^2 + \mu < 0$ and $-f/y_{Rm} < 0$. When we expand around a maximum, α becomes

$$\alpha = \alpha_m - \frac{(y_R - y_{Rm})^2 d}{2\sigma_R^2} - \frac{y_I^2 d}{2\sigma_I^2}, \tag{25}$$

in which

$$\sigma_R^2 = -d/\left(5cy_{Rm}^4 + 3by_{Rm}^2 + \mu\right) > 0 \quad \text{and} \quad \sigma_I^2 = y_{Rm}d/f > 0. \tag{26}$$

For one stable fixed point, the distribution P_s is approximately normal,

$$P_s = \frac{1}{2\pi\sigma_R\sigma_I}\exp\left[-\frac{(y_R - y_{Rm})^2}{2\sigma_R^2} - \frac{y_I^2}{2\sigma_I^2}\right], \tag{27}$$

and there are analytical expressions for its moments. Under this approximation, however, Eq. (13) no longer holds and the sign of the derivative must be found directly.

We recall that a quiescent subcritical Hopf oscillator exhibits two stable responses to tuned forcing in the deterministic limit when $9b^2/20c < \mu < 0$ and $f_1(\mu,b,c) < f < f_2(\mu,b,c)$ [Fig. 2 and Eq. (7)]. For weak noise the distribution P_s is sharply peaked around these stable fixed points at $(y_{R1},0)$ and $(y_{R2},0)$

$$P_s = \frac{\exp(\alpha_1/d)\exp\left[-\frac{(y_R-y_{R1})^2}{2\sigma_{R1}^2} - \frac{y_I^2}{2\sigma_{I1}^2}\right] + \exp(\alpha_2/d)\exp\left[-\frac{(y_R-y_{R2})^2}{2\sigma_{R2}^2} - \frac{y_I^2}{2\sigma_{I2}^2}\right]}{2\pi\left(\exp(\alpha_1/d)\sigma_{R1}\sigma_{I1} + \exp(\alpha_2/d)\sigma_{R2}\sigma_{I2}\right)}, \tag{28}$$

in which α_1 and α_2 are the values of α at the stable fixed points and the parameters are defined analogously to Eqs. (21)–(26). Because the peak value of $P_s = P_{sm} \to \infty$ as $d \to 0$, at least one $\alpha_n > 0$. The distribution is approximately the sum of two Gaussians.

For small d,

$$\frac{\partial(\langle y_R\rangle_s + \langle y_I\rangle_s)}{\partial d} = -\frac{(\alpha_1 - \alpha_2)(y_{R1} - y_{R2})\exp((\alpha_1+\alpha_2)/d)\sigma_{R1}\sigma_{I1}\sigma_{R2}\sigma_{I2}}{d^2(\exp(\alpha_1/d)\sigma_{R1}\sigma_{I1} + \exp(\alpha_2/d)\sigma_{R2}\sigma_{I2})^2} \tag{29}$$

is positive if $\alpha_1 < \alpha_2$ for $y_{R1} > y_{R2}$. This condition implies that the ratio

$$\frac{P_s(y_{R1})}{P_s(y_{R2})} = e^{\frac{\alpha_1-\alpha_2}{d}} \tag{30}$$

rises as d increases. When there are two stable responses to forcing, the phase-locked amplitude must peak when $\alpha_1 < \alpha_2$ (Fig. 2).

To find the vector strength, expansions of y_R/ρ around y_m to $O[(y - y_m)^4]$ are needed to find the dominant term for arbitrarily small d. We employ the expansion

$$\frac{y_R}{\rho} = 1 - \frac{3y_I^2}{y_{Rm}^2} + \frac{4y_I^2 y_R}{y_{Rm}^3} + \frac{3\left(y_I^4 - 4y_I^2 y_R^2\right)}{8y_{Rm}^4}. \tag{31}$$

This yields

$$\frac{\partial(\langle y_R/\rho\rangle_s + \langle y_I/\rho\rangle_s)}{\partial d} = -\frac{y_{R1}^2\exp(\alpha_2/d)\sigma_{R2}\sigma_{I2}^3 + y_{R2}^2\exp(\alpha_1/d)\sigma_{R1}\sigma_{I1}^3}{2dy_{R1}^2y_{R2}^2(\exp(\alpha_1/d)\sigma_{R1}\sigma_{I1} + \exp(\alpha_2/d)\sigma_{R2}\sigma_{I2})} < 0.$$

Due to it being a maximum in the deterministic limit, the vector strength must initially decline for small d. We confirm numerically, however, that the vector strength peaks as a function of the noise level when $\alpha_1 < \alpha_2$ (Fig. 2).

Although there is a threshold between the stable responses, stochastic resonance is evident only for operating points close to one boundary of the region possessing both responses [compare purple and orange lines in Figs. 4(c) and 4(d)]. Over a limited range, raising the noise level biases the distribution toward the fixed point at $(y_{R1},0)$ leading to an increase in entrainment.

In the subcritical case, the phase-locked amplitude can also peak as a function of the noise level when the distribution P_s has a single maximum at $(y_{Rm},0)$ (Fig. 4). In the region with a single stable fixed point and $9b^2/20c \leqslant \mu \leqslant 0$, ghosts of other fixed points exist (Fig. 2). The fixed points are defined by the zeros of the velocity vector $\mathbf{v} \equiv (\dot{y}_R, \dot{y}_I) = (0,0)$. Ghosts of fixed points are loci at which the speed $|\mathbf{v}|$ is a nonzero minimum and occur at values of y satisfying

$$\begin{aligned} \frac{\partial|\mathbf{v}|}{\partial y_R} = 0 = \frac{\partial|\mathbf{v}|}{\partial y_I}, \\ \frac{\partial^2|\mathbf{v}|}{\partial y_R^2}\frac{\partial^2|\mathbf{v}|}{\partial y_I^2} > \left(\frac{\partial^2|\mathbf{v}|}{\partial y_R y_I}\right)^2, \quad \text{and} \\ \frac{\partial^2|\mathbf{v}|}{\partial y_R^2} > 0. \end{aligned} \tag{32}$$

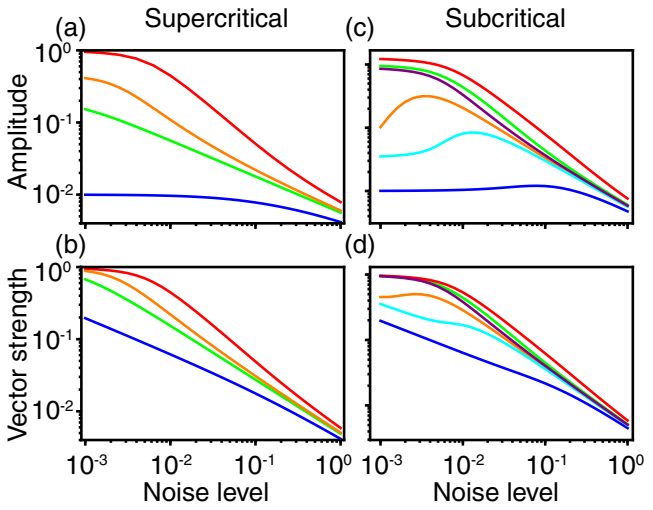

FIG. 4. The phase-locked amplitude and vector strength are shown as functions of the noise level for forcing at the Hopf frequency near supercritical [(a) and (b)] and subcritical [(c) and (d)] Hopf bifurcations. [(a) and (b)] The values of the control parameter are $\mu = 1$ (red), $\mu = 0.2$ (orange), $\mu = 0$ (green), and $\mu = -1$ (blue). [(c) and (d)] The values of the control parameter are $\mu = 1$ (red), $\mu = 0$ (green), $\mu = -0.15$ (purple), $\mu = -0.22$ (orange), $\mu = -0.3$ (cyan), and $\mu = -1$ (blue). The forcing amplitude $f = 10^{-2}$.

A ghost of a stable fixed point $(y_{\mathrm{Rv}},0)$, in which $5cy_{\mathrm{Rv}}^4 + 3by_{\mathrm{Rv}}^2 + \mu = 0$ and $y_{\mathrm{Rv}} < \sqrt{-3b/10c}$, lies on a valley of locally small speed and is separated from the stable fixed point by a ridge of locally large speed. If a stochastic fluctuation drives the system away from the stable fixed point over the pseudothreshold defined by the ridge to the region near the ghost, then for an appropriate level of noise d, the system will spend a relatively large time near the ghost due to it slowing down. Raising the noise level over a limited range can increase the probability $P_{\mathrm{s}}(y_{\mathrm{Rv}},0)$. When $f < f_1(\mu,b,c)$, $y_{\mathrm{Rv}} > y_{\mathrm{Rm}}$ and, consequently, the phase-locked amplitude can peak as a function of the noise level, but there is no peak in the vector strength [see the cyan lines in Fig. 4(c) and 4(d) for an example]. Because $y_{\mathrm{Rv}} < y_{\mathrm{Rm}}$ for $f > f_2(\mu,b,c)$, there is no stochastic resonance for larger forces [green lines in Figs. 4(c) and 4(d)].

There is, however, a sufficient condition for peaking of the phase-locked amplitude in the presence or absence of ghosts ($\mu < 9b^2/20c$). Consider either type of Hopf bifurcation under conditions for which there is a single stable response to tuned forcing. If $\langle y_{\mathrm{R}}\rangle_{\mathrm{s}} > y_{\mathrm{Rm}}$, then $\langle y_{\mathrm{R}}\rangle_{\mathrm{s}}$ peaks as a fuction of d, because $\langle y_{\mathrm{R}}\rangle_{\mathrm{s}} \to y_{\mathrm{Rm}}$ as $d \to 0$ and $\langle y_{\mathrm{R}}\rangle_{\mathrm{s}} \to 0$ as $d \to \infty$. For small d, P_{s} is sharply peaked near the stable fixed point $(y_{\mathrm{Rm}},0)$ and

$$\langle y_{\mathrm{R}}\rangle_{\mathrm{s}} \approx \int_{-\epsilon_{\mathrm{I}}}^{\epsilon_{\mathrm{I}}} dy_{\mathrm{I}} \int_{y_{\mathrm{Rm}}-\epsilon_{\mathrm{R}}}^{y_{\mathrm{Rm}}+\epsilon_{\mathrm{R}}} dy_{\mathrm{R}}\, y_{\mathrm{R}} P_{\mathrm{s}}, \tag{33}$$

in which $\epsilon_{\mathrm{R}} > 0$ and $\epsilon_{\mathrm{I}} > 0$ are finite bounds. In this limit, $\langle y_{\mathrm{R}}\rangle_{\mathrm{s}} > y_{\mathrm{Rm}}$ if

$$\int_{-\epsilon_{\mathrm{I}}}^{\epsilon_{\mathrm{I}}} dy_{\mathrm{I}} \int_{y_{\mathrm{Rm}}}^{y_{\mathrm{Rm}}+\epsilon_{\mathrm{R}}} dy_{\mathrm{R}}\, y_{\mathrm{R}} P_{\mathrm{s}} > \int_{-\epsilon_{\mathrm{I}}}^{\epsilon_{\mathrm{I}}} dy_{\mathrm{I}} \int_{y_{\mathrm{Rm}}-\epsilon_{\mathrm{R}}}^{y_{\mathrm{Rm}}} dy_{\mathrm{R}}\, y_{\mathrm{R}} P_{\mathrm{s}}, \tag{34}$$

which occurs if $\alpha(y_{\mathrm{R}},y_{\mathrm{I}}) > \alpha(2y_{\mathrm{Rm}} - y_{\mathrm{R}},y_{\mathrm{I}})$ for all $(y_{\mathrm{R}},y_{\mathrm{I}})$ satisfying $y_{\mathrm{Rm}} < y_{\mathrm{R}} < y_{\mathrm{Rm}} + \epsilon_{\mathrm{R}}$ and $-\epsilon_{\mathrm{I}} < y_{\mathrm{I}} < \epsilon_{\mathrm{I}}$.

In the supercritical case,

$$\alpha(y_{\mathrm{R}},y_{\mathrm{I}}) - \alpha(2y_{\mathrm{Rm}} - y_{\mathrm{R}},y_{\mathrm{I}}) = 2by_{\mathrm{Rm}}(y_{\mathrm{R}} - y_{\mathrm{Rm}})((y_{\mathrm{R}} - y_{\mathrm{Rm}})^2 + y_{\mathrm{I}}^2), \tag{35}$$

which is less than zero when $y_{\mathrm{Rm}} < y_{\mathrm{R}}$. There is no evidence for stochastic resonance.

For a subcritical Hopf oscillator,

$$\alpha(y_{\mathrm{R}},y_{\mathrm{I}}) - \alpha(2y_{\mathrm{Rm}} - y_{\mathrm{R}},y_{\mathrm{I}}) = 2cy_{\mathrm{Rm}}(y_{\mathrm{R}} - y_{\mathrm{Rm}})(y_{\mathrm{R}} - y_1)(y_{\mathrm{R}} + y_1 - 2y_{\mathrm{Rm}})h(y_{\mathrm{R}}), \tag{36}$$

in which $h(y_{\mathrm{R}}) > 0$ for $0 < y_{\mathrm{Rm}} < y_{\mathrm{R}}$ and $y_1 > y_{\mathrm{Rm}}$ for $y_{\mathrm{Rm}} < \sqrt{-3b/10c}$ and $|y_{\mathrm{I}}| < \sqrt{-2b/5c}$. By choosing $\epsilon_{\mathrm{I}} < \sqrt{-2b/5c}$ and ϵ_{R} such that $y_{\mathrm{Rm}} < y_{\mathrm{R}} < y_{\mathrm{Rm}} + \epsilon_{\mathrm{R}} < y_1$ we can ensure $\alpha(y_{\mathrm{R}},y_{\mathrm{I}}) - \alpha(2y_{\mathrm{Rm}} - y_{\mathrm{R}},y_{\mathrm{I}}) > 0$ for $y_{\mathrm{Rm}} < y_{\mathrm{R}} < y_{\mathrm{Rm}} + \epsilon_{\mathrm{R}}$ and $-\epsilon_{\mathrm{I}} < y_{\mathrm{I}} < \epsilon_{\mathrm{I}}$. Using $cy_{\mathrm{Rm}}^5 + by_{\mathrm{Rm}}^3 + \mu y_{\mathrm{Rm}} + f = 0$ [Eq. (23)], we find $y_{\mathrm{Rm}} < \sqrt{-3b/10c}$ when $f < f_4(\mu,b,c)$, in which

$$f_4(\mu,b,c) = \sqrt{\frac{-3b}{10c}}\left(\frac{21b^2 - 100c\mu}{100c}\right). \tag{37}$$

Because $f_1(\mu,b,c) \leqslant f_4(\mu,b,c)$ when $9b^2/20c \leqslant \mu < b^2/4c$, this sufficient condition for peaking of the phase-locked response also holds when ghosts of other fixed points exist. Stochastic resonance for tuned forcing arises from the asymmetric redistribution of P_{s} as d grows and does not occur when $\mu > 0$ or for large forcing amplitudes [Fig. 2 and Fig. 4(c)].

2. Stochastic resonance is possible near supercritical and subcritical Hopf bifurcations in response to detuned forcing

A deterministic supercritical Hopf oscillator is perfectly entrained by sinusoidal forcing when the frequency detuning is small or the forcing amplitude is big [Fig. 5(a)]. For weak forcing or large detuning, the system in the frame rotating at the driving frequency exhibits a stable limit cycle surrounding an unstable fixed point [Fig. 5(b)]. The response amplitude y varies with time, corresponding to less-than-perfect entrainment. In this regime, we show that noise can increase the system's response to forcing.

We first introduce the angular distribution

$$P_{\psi}(\psi) = \int_0^{\infty} P_{\mathrm{ps}}(\rho,\psi)\, d\rho, \tag{38}$$

knowledge of which is sufficient to calculate the vector strength

$$V = |\langle e^{i\psi}\rangle_{\mathrm{s}}| = \left|\int_0^{2\pi} e^{i\psi} P_{\psi}(\psi)\, d\psi\right|. \tag{39}$$

For arbitrarily small noise, the peak of the angular distribution corresponds to a minimum in the deterministic system's speed on the limit cycle [Fig. 5(c)]. Raising the noise level reduces the peak and shifts the peak angle toward zero in accordance with the behavior of the detuned distribution $P_{s\delta\omega}(y)$. The change in the angular distribution with noise level and the associated stochastic resonance can be understood by considering the behavior of a simpler system.

For sufficiently weak noise and in the long-time limit, the forced system's dynamics can be captured by a single variable defining its position along the limit cycle. To construct a similar

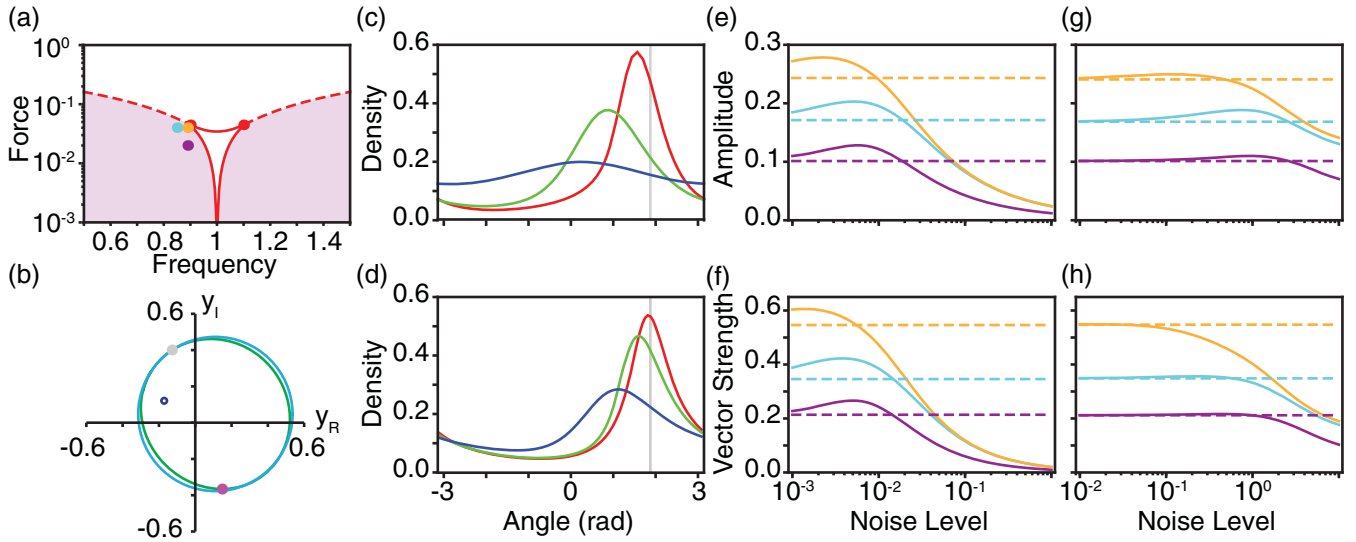

FIG. 5. Stochastic resonance for a self-oscillating ($\mu = 0.2 \geqslant 0$) and detuned supercritical Hopf oscillator. (a) The state of a deterministic oscillator is a function of the forcing amplitude and frequency. Areas of less than perfect entrainment (light purple regions) are separated from those exhibiting perfect entrainment (white regions) by supercritical Hopf (dashed red lines) or a saddle-node (solid red lines) bifurcations, which meet tangentially at Bogdanov-Takens points (red dots). Global bifurcations are not shown. Dots indicate the operating points ($\omega = 0.89, f = 4 \times 10^{-2}$) (orange), ($\omega = 0.85, f = 4 \times 10^{-2}$) (cyan), and ($\omega = 0.89, f = 2 \times 10^{-2}$) (purple). (b) At the orange operating point a stable limit cycle (dark green) surrounds an unstable fixed point (dark blue). The speed on the cycle is a minimum (maximum) at the gray (magenta) point. A circular locus with the same center as the limit cycle and passing through the cycle's point of minimum speed is shown (light blue). (c) Angular probability distributions $P_\psi(\psi)$ for the orange operating point are shown for the noise levels $d = 10^{-3}$ (red), $d = 10^{-2}$ (green), and $d = 10^{-1}$ (blue). The deterministic system resides for the greatest time at the limit cycle's point of minimum speed (gray line). (d) Adler dynamics along the light blue circle in (b) ($A = 1.19$) yields the probability distributions $P_A(\psi)$ for the noise levels $d_A = 10^{-2}$ (red), $d_A = 10^{-1}$ (green), and $d_A = 10^{0}$ (blue). The Adler system's speed is chosen to be a minimum at the same angle for which the speed on the limit cycle is a minimum (gray line). [(e)–(h)] The phase-locked amplitude and vector strength are shown as functions of the noise level (solid lines) and in the deterministic limit (dashed lines). [(e) and (f)] Responsiveness for operating points indicated in (a). [(g) and (h)] Responsiveness for Adler dynamics on circular loci matched to the operating points indicated in (a); $A = 1.19$ (orange), $A = 1.65$ (cyan), and $A = 2.5$ (purple).

but simpler system, we define a circular locus $y_A = y_{RA} + i y_{IA}$ with the same center as the limit cycle, in which

$$\begin{aligned} y_{RA} &= y_{Rc} + R_A \cos(\beta + \beta_0) \quad \text{and} \\ y_{IA} &= y_{Ic} + R_A \sin(\beta + \beta_0). \end{aligned} \tag{40}$$

The center of the circle is defined by

$$\begin{aligned} y_{Rc} &= \left[\max_{cyc}(y_R) + \min_{cyc}(y_R)\right]/2 \quad \text{and} \\ y_{Ic} &= \left[\max_{cyc}(y_I) + \min_{cyc}(y_I)\right]/2, \end{aligned} \tag{41}$$

in which the extrema are taken over the limit cycle [Fig. 5(b)]. The radius R_A is fixed by requiring that the circle passes through the point for which the Hopf system's speed is a minimum on the limit cycle. To describe the dynamics of β, we employ the Adler equation

$$\dot{\beta} = A - \sin\beta \tag{42}$$

and choose β_0 such that $\dot{\beta}$ is a minimum at the same coordinate for which the Hopf system's speed is a minimum on the limit cycle. In each interval $[n\pi,(n+2)\pi]$ of β, $n \in \mathbb{Z}$, the Adler system has a stable fixed point and an unstable fixed point when $|A| < 1$. No fixed points exist when $|A| > 1$. Neglecting transients, the solution of Eq. (42) up to a multiple of 2π is

$$\beta(t) = 2\arctan\left[\frac{1 - \sqrt{A^2-1}\tan(-t\sqrt{A^2-1}/2)}{A}\right]. \tag{43}$$

The corresponding Fokker-Plank equation,

$$\partial_t P_A = -\partial_\beta[(A - \sin\beta)P_A - d_A \partial_\beta P_A], \tag{44}$$

has the steady-state solution

$$P_{As} = N_A e^{\frac{A\beta+\cos\beta-1}{d_A}}\left(\int_0^\beta e^{-\frac{A\beta'+\cos\beta'-1}{d_A}}\,d\beta' + e^{\frac{2\pi A}{d_A}}\int_\beta^{2\pi} e^{-\frac{A\beta'+\cos\beta'-1}{d_A}}\,d\beta'\right), \tag{45}$$

in which d_A is the noise level and N_A is a normalization factor. The steady-state angular distribution is defined by

$$P_{\psi_C}[\psi_C(\beta)] = P_{As}(\beta), \tag{46}$$

in which $\psi_C(\beta) = \arg(y_A(\beta))$.

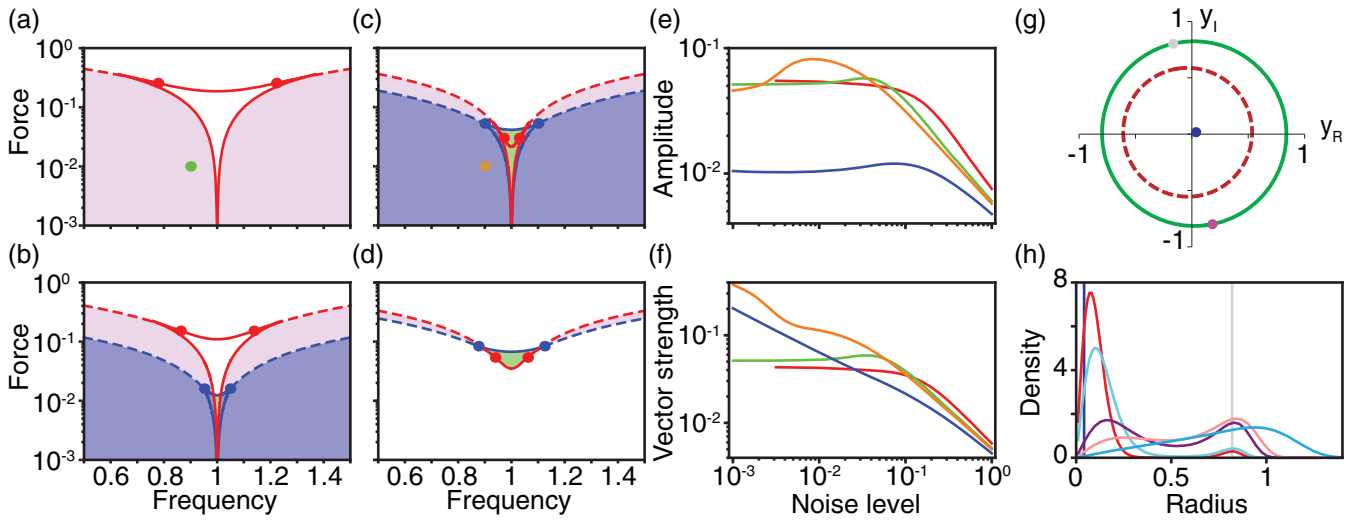

FIG. 6. Stochastic resonance for a detuned subcritical Hopf oscillator. [(a)–(d)] State diagrams for a deterministic system as functions of the forcing amplitude and stimulus frequency are depicted similarly to Fig. 5(a). The forced oscillator is perfectly entrained when it possesses one stable fixed point in the white regions or two stable fixed points in the central green regions. Less than perfect entrainment occurs when the system possesses an unstable fixed point and a stable limit cycle (light purple regions) or a stable fixed point coexisting with a stable and unstable limit cycle (blue regions). (a) The state diagram for $\mu \geqslant 0$ ($\mu = 0$) is illustrated. The Hopf bifurcations are supercritical. (b) The diagram corresponding to $b^2/5c < \mu < 0$ ($\mu = -0.1$) is shown. The red (blue) Hopf bifurcation lines are supercritical (subcritical). (c) The state diagram for $b^2/4c < \mu < b^2/5c$ ($\mu = -0.22$) is similar to (b) except that the central red line dips below the central blue line. (d) The state diagram when $9b^2/20c < \mu < b^2/4c$ ($\mu = -0.3$) is depicted. The Hopf bifurcations illustrated are supercritical. [(e) and (f)] The detuned ($\omega = 0.9\,\omega_0$) phase-locked amplitude and vector strength are shown as functions of the noise level. The values of the control parameter are $\mu = 1$ (red), $\mu = 0$ (green, indicated in panel a), $\mu = -0.22$ [orange, indicated in (c)], and $\mu = -1$ (blue). The forcing amplitude $f = 10^{-2}$. (g) At the orange operating point in (c), a stable limit cycle (dark green) surrounds an unstable limit cycle (dashed red line), which encloses a stable fixed point (dark blue dot). The points at which the speed on the stable limit cycle is a minimum (gray) and maximum (magenta) are shown. (h) Amplitude distributions $P_\rho(\rho)$ for the orange point are shown in which the noise level $d = 10^{-3}$ (dark red), $d = 2 \times 10^{-3}$ (cyan), $d = 5 \times 10^{-3}$ (purple), $d = 10^{-2}$ (light red), and $d = 10^{-1}$ (light blue). The vertical dark blue (gray) line corresponds to the stable fixed point (point of minimum speed on the stable limit cycle) shown in (g).

For each operating point of the forced Hopf oscillator, we can construct a circular locus with Adler dynamics that captures some of the oscillator's basic behavior. The deterministic phase-locked amplitude and vector strength are calculated as before using Eqs. (40) and (43). We choose the value of A in each case such that the deterministic limits for the vector strengths of the Hopf oscillator and the circular Adler system are approximately equal. The stochastic phase-locked response is given by

$$\left| \int_0^{2\pi} y_A(\beta) P_{\mathrm{As}}(\beta)\, d\beta \right| \tag{47}$$

and the stochastic vector strength is

$$\left| \int_0^{2\pi} e^{i\psi_{\mathrm{C}}(\beta)} P_{\mathrm{As}}(\beta)\, d\beta \right|. \tag{48}$$

Similarly to the Hopf oscillator, the peak of the angular distribution on the circular locus decreases and moves to $\psi_{\mathrm{C}} = 0$ as the noise level rises [Fig. 5(d)]. This behavior is determined by Eq. (45) as the peak of P_{As} shifts to $\beta = 0$ as $d_{\mathrm{A}} \to 0$.

When the forced deterministic oscillator exhibits a limit cycle, the phase-locked amplitude and vector strength of the Hopf oscillator peak as functions of the noise level [Figs. 5(e) and 5(f)]. The peaks diminish and move to higher levels of noise as the detuning is increased or the forcing amplitude is decreased. The circular Adler system exhibits the same qualitative changes with noise level [Fig. 5(g) and 5(h)]. Peaks do not occur, however, if the circular locus is centered at (0,0) instead of at $(y_{\mathrm{Rc}}, y_{\mathrm{Ic}})$. Stochastic resonance in the supercritical Hopf oscillator stems from the noncircular redistribution of the probability density with increasing noise.

A deterministic subcritical Hopf oscillator possesses four distinct state diagrams as functions of the forcing amplitude and stimulus frequency (Fig. 6). In the self-oscillating scenario [Fig. 6(a)], the diagram is qualitatively similar to that of a supercritical oscillator and the subcritical Hopf oscillator operating within the purple zones exhibits stochastic resonance arising from the same mechanism [green lines in Figs. 6(e) and 6(f)]. This mechanism also applies to operating points in the light purple sectors of Figs. 6(b) and 6(c).

For sufficiently small detuning, the forced oscillator is qualitatively similar to the tuned case, in which two stable responses are associated with peaks in the responsiveness as a function of the noise level [central green areas in Figs. 6(b)–6(d)]. Like a resonantly forced oscillator, the phase-locked amplitude can also peak as a function of the noise level when there is a single stable response [blue line in Fig. 6(e)].

In two of the state diagrams [blue regions in Figs. 6(b) and 6(c)], stochastic resonance can arise from yet another mechanism, in which a stable fixed point is separated from

a stable limit cycle by an unstable limit cycle [Fig. 6(g)]. In the deterministic limit, whether an oscillator is perfectly entrained depends on the initial conditions. For weak noise, the system's probability density possesses two peaks, a large peak near the stable fixed point and a smaller peak near the point of minimum speed on the stable limit cycle. The radial distribution

$$P_\rho(\rho) = \int_0^{2\pi} P_{\rm ps}(\rho,\psi)\,d\psi \tag{49}$$

also peaks near radii defined by these points [Fig. 6(h)]. The stable fixed point is associated with a greater degree of entrainment than the stable limit cycle. As the noise level increases from zero, the peak near the stable fixed point moves to a larger radial value and decreases in amplitude, but this peak still dominates the distribution. Consequently, the phase-locked amplitude grows with the noise level. For sufficiently large noise levels, however, the density is greatest near the limit cycle and the phase-locked amplitude is correspondingly diminished. The distribution has a single peak for very large noise levels, in which the noise obscures the system's deterministic structure. Although the most probable value of ρ grows for very large noise levels, the phase-locked amplitude declines.

III. DISCUSSION

Stochastic resonance and coherence resonance have been demonstrated using a variety of measures from power spectra to residence-time distributions [2,24]. Coherence resonance has been analyzed and observed experimentally for several systems operating near a Hopf bifurcation and has been demonstrated for the normal form of a subcritical Hopf oscillator with additive noise [21,25–27]. Here we distinguish coherence resonance from stochastic resonance by employing the phase-locked amplitude and vector strength, which are zero in the absence of deterministic forcing.

Despite the simplicity of the system we study, we find multiple distinct mechanisms for stochastic resonance. In all cases, the redistribution of the probability density as the noise level increases depends on the underlying structure of the deterministic system. We show that a peak in the phase-locked amplitude does not imply a maximum in the vector strength and that, when both quantities peak, they do so at distinct noise levels.

First, two stable responses to forcing for a tuned or weakly detuned subcritical Hopf oscillator lead to peaks in the phase-locked amplitude and vector strength as functions of the noise level. We show, however, that the existence of two stable fixed points does not imply stochastic resonance and find analytical expressions for the boundaries of the region in parameter space in which this type of resonance takes place.

Second, for a tuned or weakly detuned subcritical oscillator, the phase-locked amplitude can peak as a function of the noise level without peaking in the vector strength. Analytical expressions can be found defining a set of operating points for which a single stable fixed point is associated with stochastic resonance in the phase-locked amplitude. This resonance arises from the residual influence of a pair of fixed points, a stable fixed point and a saddle point that were annihilated through a saddle-node bifurcation, on the deterministic vector field.

Third, spontaneously oscillating supercritical and subcritical Hopf oscillators display stochastic resonance in the phase-locked amplitude and vector strength in response to detuned, weak forcing. We show that simple phase dynamics on a circular limit cycle can explain this type of resonance if the cycle possesses an asymmetry with respect to the phase coordinate. Placing the center of the circular cycle away from the Cartesian origin is sufficient to generate peaks in both responsiveness measures.

Fourth, a subcritical Hopf oscillator possesses a stable fixed point, an unstable limit cycle, and a stable limit cycle for a limited set of control parameter values. As the noise level is raised, the most probable state of the system shifts from being near the stable fixed point to residing close to the stable limit cycle. Before this transition, the phase-locked amplitude, but not the vector strength, peaks as a function of the noise level.

Stochastic resonance has been demonstrated on both sides of a supercritical Hopf bifurcation [3–6,28,29]. In these cases, the systems studied have features absent from the Hopf oscillators we describe. For example, rapid changes in the amplitude of spontaneous oscillations with control parameter, known as canard explosions, occur [30], the resonant frequency varies with control parameter and forcing amplitude [18,19], there are multiple stable responses at a single stimulus frequency [18,19], and the noise is not additive, Gaussian, or white in the normal-form coordinate system [16,23,31]. We restrict our analysis to $b' = 0$ and additive, Gaussian, white noise and do not find stochastic resonance on the stable side of the bifurcation. The difference may simply stem, however, from our use of responsiveness measures different from these previous reports. Stochastic resonance has also been reported in systems close to subcritical Hopf bifurcations [7–9]. It is unclear whether these resonances can be ascribed to a particular feature of each system or to one of the generic mechanisms described here.

The phase-locked amplitude and vector strength capture two different aspects of a system's response to driving. Stochastic resonance in the vector strength shows that noise can improve phase locking to the stimulus. In comparison, a peak in the phase-locked amplitude as a function of the noise level illustrates that noise can augment the response amplitude and phase locking to the input. In two of the mechanisms we describe, noise boosts the phase-locked amplitude more than the degree of entrainment.

Although the stochastic enhancement we find is sometimes only a fraction of the deterministic limit, stochastic resonance can mean the difference between a signal being detected or not. For example, the threshold of hearing corresponds to vibrations in the ear of less than a nanometer measured over time scales of less than a second [32]. In this noise-dominated regime, it is possible that fractional increases in the phase-locked amplitude or vector strength due to noise could determine the threshold. Stochastic resonance in some systems may simply be the consequence of their operation near a Hopf bifurcation, which can be ensured by an additional feedback mechanism [33].

ACKNOWLEDGMENTS

We thank A. J. Hudspeth for support and Andrew R. Milewski for constructive comments on the manuscript.

APPENDIX: DETERMINISTIC LIMIT

In polar coordinates $y = \rho e^{i\psi}$, and Eq. (2) becomes

$$\begin{aligned} \dot{\rho} &= \mu\rho + b\rho^3 + c\rho^5 + f\cos\psi, \\ \dot{\psi} &= -\delta\omega + b'\rho^2 + c'\rho^4 - \frac{f\sin\psi}{\rho}, \end{aligned} \tag{A1}$$

in the deterministic limit. The fixed points ρ^* and ψ^* then satisfy

$$(\mu + b\rho^{*2} + c\rho^{*4})^2\rho^{*2} + (-\delta\omega + b'\rho^{*2} + c'\rho^{*4})^2\rho^{*2} = f^2, \tag{A2}$$

and their linear stability is determined by the eigenvalues of the Jacobian

$$\mathbf{J} \equiv \begin{pmatrix} \mu + 3b\rho^{*2} + 5c\rho^{*4} & \delta\omega\rho^* - b'\rho^{*3} - c'\rho^{*5} \\ -\frac{\delta\omega}{\rho^*} + 3b'\rho^* + 5c'\rho^{*3} & \mu + b\rho^{*2} + c\rho^{*4} \end{pmatrix}. \tag{A3}$$

A local bifurcation can occur when either the trace of **J** is zero while the determinant of **J** is positive definite or when the determinant is zero.

In the isochronous case $b' = c' = 0$ and for tuned forcing $\delta\omega = 0$, Eq. (A2) becomes

$$\left(\mu + by_{\mathrm{R}}^{*2} + cy_{\mathrm{R}}^{*4}\right)^2 y_{\mathrm{R}}^{*2} = f^2, \tag{A4}$$

in which $\psi^* = 0$ or π such that $y_{\mathrm{I}}^* = 0$. Saddle-node bifurcations occur when the determinant of **J** is zero or, equivalently, when $\mu + 3by_{\mathrm{R}}^{*2} + 5cy_{\mathrm{R}}^{*4} = 0$ (Fig. 2).

In a deterministic system, perfect phase locking is defined to occur when the amplitude of the response ρ and the phase difference between the response and driving ψ are independent of time. For a quiescent Hopf oscillator, perfect phase locking occurs for all forcing amplitudes and frequencies. A resonantly forced self-oscillating system exhibits perfect phase locking at all forcing amplitudes.

When there is detuning, sufficiently high forces are required to perfectly phase lock an oscillating system. The range of the forces for which perfect phase locking occurs can be found as a function of the stimulus frequency as long as the forcing is not too large [20]. A state diagram of the forced system is determined by lines of local bifurcations from Eq. (A3) (Figs. 5 and 6). These bifurcation lines demarcate the region of perfect phase locking, which is narrower than the 1:1 Arnold tongue.

[1] Y. Choe, M. O. Magnasco, and A. J. Hudspeth, Proc. Natl. Acad. Sci. U.S.A. **95**, 15321 (1998).
[2] L. Gammaitoni, P. Hänggi, P. Jung, and F. Marchesoni, Rev. Mod. Phys. **70**, 223 (1998).
[3] A. Longtin, J. Stat. Phys. **70**, 309 (1993).
[4] X. Pei, K. Bachmann, and F. Moss, Phys. Lett. A **206**, 61 (1995).
[5] V. V. Osipov and E. V. Ponizovskaya, JETP Lett. **70**, 425 (1999).
[6] V. V. Osipov and E. V. Ponizovskaya, Phys. Rev. E **61**, 4603 (2000).
[7] W. Hohmann, J. Müller, and F. W. Schneider, J. Phys. Chem. **100**, 5388 (1996).
[8] S. Reinker, E. Puil, and M. R. Miura, Bull. Math. Biol. **65**, 641 (2003).
[9] M. Perc and M. Marhl, Physica A **332**, 123 (2004).
[10] I. L'Heureux, in *Advances in Nonlinear Geosciences*, edited by A. A. Tsonis (Springer International, Cham, 2018), pp. 143–160.
[11] Y. A. Kuznetsov, *Elements of Applied Bifurcation Theory*, 2nd ed. (Springer-Verlag, New York, 1998).
[12] J. Guckenheimer and P. Holmes, *Nonlinear Oscillations, Dynamical Systems, and Bifurcations of Vector Fields*, 1st ed. (Springer, New York, 1983).
[13] S. H. Strogatz, *Nonlinear Dynamics and Chaos* (Perseus Books, Reading, Massachusetts, 1994).
[14] R. L. Stratonovich, *Topics In the Theory of Random Noise* (Gordon & Breach, London, 1967), Vol. 2.
[15] J. P. Gleeson and F. O'Doherty, SIAM J. Appl. Math. **66**, 1669 (2006).
[16] F. Jülicher, K. Dierkes, B. Lindner, J. Prost, and P. Martin, Eur. Phys. J. E **29**, 449 (2009).
[17] C. W. Gardiner, *Handbook of Stochastic Methods: For Physics, Chemistry and the Natural Sciences*, 3rd ed. (Springer-Verlag, New York, 2004).
[18] Y. Zhang and M. Golubitsky, SIAM J. Appl. Dynam. Sys. **10**, 1272 (2011).
[19] J. Wiser and M. Golubitsky, SIAM J. Appl. Dynam. Sys. **14**, 2013 (2015).
[20] A. Pikovsky, M. Rosenblum, and J. Kurths, *Synchronization (A Universal Concept in Nonlinear Sciences)*, 1st ed. (Cambridge University Press, Cambridge, 2003).
[21] O. V. Ushakov, H.-J. Wünsche, F. Henneberger, I. A. Khovanov, L. Schimansky-Geier, and M. A. Zaks, Phys. Rev. Lett. **95**, 123903 (2005).
[22] R. D. Hempstead and M. Lax, Phys. Rev. **161**, 350 (1967).
[23] L. Arnold, *Random Dynamical Systems*, 1st ed. (Springer, New York, 2003).
[24] B. Lindner, J. García-Ojalvob, A. Neimand, and L. Schimansky-Geier, Phys. Rep. **392**, 321 (2004).
[25] V. Osipov and E. Ponizovskaya, Phys. Lett. A **238**, 369 (1998).
[26] I. A. Khovanov, L. Schimansky-Geier, and M. A. Zaks, Acta Phys. Pol. B **37**, 1551 (2006).
[27] A. Zakharova, A. Feoktistov, T. Vadivasova, and E. Schöll, Eur. Phys. J. Spec. Top. **222**, 2481 (2013).
[28] A. Guderian, G. Dechert, K.-P. Zeyer, and F. W. Schneider, J. Phys. Chem. **100**, 4437 (1996).
[29] J. P. Baltanás and J. M. Casado, Phys. Rev. E **65**, 041915 (2002).
[30] E. M. Izhikevich, *Dynamical Systems in Neuroscience: The Geometry of Excitability and Bursting* (The MIT Press, Cambridge, MA, 2007).
[31] P. Coullet, C. Elphick, and E. Tirapegui, Phys. Lett. A **111**, 277 (1985).
[32] T. Ren, W. He, and D. Kemp, Proc. Natl. Acad. Sci. U.S.A. **113**, 9910 (2016).
[33] A. R. Milewski, D. Ó Maoiléidigh, J. D. Salvi, and A. J. Hudspeth, Proc. Natl. Acad. Sci. U.S.A. **114**, E6794 (2017).